

Combined parametrization of G_{En} and $\gamma^*N \rightarrow \Delta(1232)$ quadrupole form factors

G. Ramalho

Laboratório de Física Teórica e Computacional – LFTC, Universidade Cruzeiro do Sul, 01506-000, São Paulo, SP, Brazil

Received: date / Revised version: date

Abstract. Models based on $SU(6)$ symmetry breaking and large N_c limit provide relations between the pion cloud contributions to the $\gamma^*N \rightarrow \Delta(1232)$ quadrupole form factors, electric (G_E) and Coulomb (G_C), and the neutron electric form factor G_{En} , suggesting that those form factors are dominated by the same physical processes. Those relations are improved in order to satisfy a fundamental constraint between the electric and Coulomb quadrupole form factors in the long wavelength limit, when the photon three-momentum vanishes (Siegert's theorem). Inspired by those relations, we study alternative parametrizations for the neutron electric form factor. The parameters of the new form are then determined by a combined fit to the G_{En} and the $\gamma^*N \rightarrow \Delta(1232)$ quadrupole form factor data. We obtain a very good description of the G_E and G_C data when we combine the pion cloud contributions with small valence quark contributions to the $\gamma^*N \rightarrow \Delta(1232)$ quadrupole form factors. The best description of the data is obtained when the second momentum of G_{En} is $r_n^4 \simeq -0.4 \text{ fm}^4$. We conclude that the square radii associated with G_E and G_C , r_E^2 and r_C^2 , respectively, are large, revealing the long extension of the pion cloud. We conclude also that those square radii are related by $r_E^2 - r_C^2 = 0.6 \pm 0.2 \text{ fm}^2$. The last result is mainly the consequence of the pion cloud effects and Siegert's theorem.

PACS. 13.40.Gp Electromagnetic form factors – 14.20.Gk Baryon resonances with $S=0$ – 14.20.Dh Protons and neutrons

1 Introduction

Among all the nucleon excitations the $\Delta(1232)$ plays a special role, not only because it is a spin 3/2 system with the same quark content as the nucleon, but also because it is very well known experimentally [1, 2, 3]. The electromagnetic transition between the nucleon (N) and the $\Delta(1232)$ is characterized by the magnetic dipole form factor (G_M) and two quadrupole form factors: the electric (G_E) and the Coulomb (G_C) form factors [4]. The magnetic dipole is the dominant form factor, as expected from the quark spin-flip transition [5, 6, 7, 8, 9, 10, 11, 12, 13, 14], while the quadrupole form factors are small, but non-zero [1, 2, 15, 16, 17, 18, 19, 20]. The transition form factors are traditionally represented in terms of $Q^2 = -q^2$, where q is the $\gamma^*N \rightarrow \Delta(1232)$ momentum transfer, or photon momentum. Experimental data are available only in the region $Q^2 \geq 0$.

The non-zero results for the quadrupole form factors are the consequence of asymmetries on the $\Delta(1232)$ structure, which implies the deviation of the $\Delta(1232)$ from a spherical shape [2, 6, 16, 21, 22, 23, 24, 25, 26, 27, 28]. Estimates of the electric and Coulomb quadrupole form factors based on valence quark degrees of freedom can explain in general only a small fraction of the observed data [2, 6, 7, 16, 25, 29, 30, 31, 32]. The strength, missing in quark models

can be explained when we take into account the quark-antiquark effects in the form of meson cloud contributions [29, 30, 31, 32, 33, 34, 35, 36].

Calculations based on non relativistic $SU(6)$ quark models with symmetry breaking and large N_c limit show that the $\gamma^*N \rightarrow \Delta(1232)$ quadrupole form factors are dominated by pion cloud effects at small Q^2 ($Q^2 < 1 \text{ GeV}^2$) [2, 23, 33, 37, 38, 39, 40]. Simple parametrizations of the pion cloud contributions to the quadrupole form factors G_E and G_C , labeled as G_E^π and G_C^π , respectively, have been derived using the large N_c limit [33], in close agreement with the empirical data [33, 41]. Those parametrizations relate G_E^π and G_C^π with the neutron electric form factor [33, 38, 39], and are discussed in sect. 2.

There are some limitations associated with the use of those pion cloud parametrizations: they underestimate the $Q^2 < 0.2 \text{ GeV}^2$ data by about 10-20% [19, 20, 41, 42], and they are in conflict with Siegert's theorem, a fundamental constraint between the quadrupole form factors also known as the long wavelength limit [19, 20, 43, 44, 45, 46].

Siegert's theorem states that at the pseudothreshold, when $Q^2 = Q_{pt}^2 \equiv -(M_\Delta - M)^2$, one has [4, 19, 20, 42, 47]

$$G_E(Q_{pt}^2) = \kappa G_C(Q_{pt}^2), \quad (1)$$

where M and M_Δ are the nucleon and $\Delta(1232)$ masses, respectively, and $\kappa = \frac{M_\Delta - M}{2M_\Delta}$. The pseudothreshold is

the point where the photon three-momentum \mathbf{q} , vanishes ($|\mathbf{q}| = 0$), and the nucleon and the $\Delta(1232)$ are both at rest.

Concerning Siegert's theorem, the problem can be solved correcting the parametrization for G_E^π with a term $\mathcal{O}(1/N_c^2)$ at the pseudothreshold, as shown recently in [20]. Concerning the underestimation of the data associated with the quadrupole form factors G_E and G_C , it can be partially solved with the addition of contributions to those form factors associated with the valence quarks. Although small, those contributions move the estimates based on the pion cloud effects in the direction of the measured data [7, 18, 19, 30, 31].

In the previous picture, there is only a small setback, the combination of pion cloud and valence quark contributions is unable to describe the previous Coulomb quadrupole form factor data below 0.2 GeV² [19]. However, it has been shown recently that the previous extractions of G_C data at low Q^2 ($Q^2 < 0.2$ GeV²) overestimate the actual values of the form factor [41], and that the new results are in excellent agreement with the estimates based on the pion cloud parametrizations [20].

The main motivation for this work is to check if there are parametrizations of G_{En} which optimizes the description of the G_E and G_C data and provides at the same time an accurate description of the neutron electric form factor data. With this goal in mind, we perform a global fit of the functions G_{En} , G_E^π and G_C^π , to the experimental form factor data, based on the pion cloud parametrization of the quadrupole form factors. An accurate description of the data indicates a correlation between the pion cloud effects in the neutron and in the $\gamma^*N \rightarrow \Delta(1232)$ transition [33]. In addition, a global fit, which includes the G_E and G_C data, can help to constrain the shape of G_{En} , since the neutron electric form factor data have in general large error bars.

The main focus of the present work is then on the parametrization of the function G_{En} . In the past, simplified parametrizations of G_{En} with a small number of parameters have been used. Examples of these parametrizations, are, the Galster parametrization, and the Bertozzi parametrization, based on the differences of two poles, among others [48, 49, 50, 51, 52, 53, 54]. More sophisticated parametrizations, with a larger number of parameters have been derived based on dispersion relations and chiral perturbation theory [55, 56, 57, 58]. For the purpose of the present work, however, it is preferable to use simple expressions with a small number of parameters. We propose then a parametrization of G_{En} with three parameters.

The parametrizations of G_{En} can also be analyzed in terms of first moments of the expansion of G_{En} near $Q^2 = 0$, namely, the first (r_n^2), the second (r_n^4) and the third (r_n^6) moments. The explicit definitions are presented in sect. 3. In the present work, motivated by a previous study of the $\gamma^*N \rightarrow \Delta(1232)$ quadrupole form factors and their relations with Siegert's theorem [19], we consider a parametrization of G_{En} based on rational functions. Those parametrizations have a simple form for low Q^2 and are also compatible with the expected falloff at

large Q^2 . Alternative parametrizations based on rational functions can be found in [19, 59].

As mentioned above, the description of the G_E and G_C data can be improved when we include additional contributions associated with the valence quark component. Inspired by previous works, where the valence quark contributions are estimated based on the analysis of the results from lattice QCD [9, 18, 19], we include in the present study the valence quark contributions calculated with the covariant spectator quark model from [18]. The model under discussion is covariant and consistent with lattice QCD results [8, 18, 60]. Since in lattice QCD simulations with large pion masses the meson contributions are suppressed, the physics associated with the valence quarks can be calibrated more accurately within the model uncertainties [9]. An additional advantage in the use of a quark model framework is that the G_E and G_C form factors are identically zero at the pseudothreshold, as a consequence of the orthogonality between the nucleon and $\Delta(1232)$ states [18, 19]. This point is fundamental for the consistence of the present model with the constraints of Siegert's theorem.

We conclude at the end, that the combination of the G_{En} , G_E and G_C data does help to improve the accuracy of the parametrization of G_{En} (small errors associated with the parameters). The best description of the data is obtained when the second moment of G_{En} , r_n^4 is about -0.38 fm⁴. A consequence of this result is that the square radii associated with G_E and G_C (r_E^2 and r_C^2) are large, suggesting a long spacial extension of the pion cloud (or quark-antiquark distribution) for both form factors. We conclude also that, as a consequence of the pion cloud parametrizations of the G_E and G_C quadrupole form factors, one obtains $r_E^2 - r_C^2 = 0.6 \pm 0.2$ fm². The uncertainties of the estimates are also discussed.

This article is organized as follows: In the next section, we discuss the pion cloud parametrizations of the $\gamma^*N \rightarrow \Delta(1232)$ quadrupole form factors. In sect. 3, we discuss our parametrization of the neutron electric form factor. In sect. 4, we present the results of the global fit to the G_{En} , G_E and G_C data, and discuss the physical consequences of the results. The outlook and conclusions are presented in sect. 5.

2 Pion cloud parametrization of G_E and G_C

The internal structure of the baryons can be described using a combination $SU(6)$ quark models with two-body exchange currents and the large N_c limit [37, 38, 39]. The $SU(6)$ symmetry breaking induces an asymmetric distribution of charge in the nucleon and $\Delta(1232)$ systems, which is responsible for the non-vanishment of the neutron electric form factor and for the non-zero results for the $\gamma^*N \rightarrow \Delta(1232)$ quadrupole moments [39]. Those results can be derived in the context of constituent quark models as the Isgur-Karl model [61, 62, 63], and others [2, 23, 38]. More specifically, we can conclude, based on the $SU(6)$ symmetry breaking, that the $\gamma^*N \rightarrow \Delta(1232)$ quadrupole moments are proportional to the neutron electric square

radius (r_n^2). Based on similar arguments, we can also relate the electric quadrupole moment of the $\Delta(1232)$ and other baryons, with the neutron electric square radius [23, 24, 40, 64, 65, 66]. From the large N_c framework, we can conclude that when $Q^2 = 0$, one has $\frac{G_E}{G_M} = \mathcal{O}(\frac{1}{N_c^2})$ and $G_E = \frac{M_\Delta^2 - M^2}{4M_\Delta^2} G_C$ [2, 67].

The derivation of the pion cloud contribution to the $\gamma^*N \rightarrow \Delta(1232)$ quadrupole form factors are based on relations between the quadrupole moments and the neutron electric square radius, discussed above, and on the low- Q^2 expansion of the neutron electric form factor: $G_{En} \simeq -\frac{1}{6}r_n^2 Q^2$ [23, 33, 37, 38, 39, 40]. One can then write

$$G_E^\pi(Q^2) = \left(\frac{M}{M_\Delta}\right)^{3/2} \frac{M_\Delta^2 - M^2}{2\sqrt{2}} \frac{\tilde{G}_{En}(Q^2)}{1 + \frac{Q^2}{2M_\Delta(M_\Delta - M)}}, \quad (2)$$

$$G_C^\pi(Q^2) = \left(\frac{M}{M_\Delta}\right)^{1/2} \sqrt{2} M_\Delta M \tilde{G}_{En}(Q^2), \quad (3)$$

where $\tilde{G}_{En} = G_{En}/Q^2$.

The interpretation of the previous relations as representative of the pion cloud contributions is a consequence of the connection between quadrupole form factors and r_n^2 . Those relations have been derived in the framework of the constituent form factors with two-body exchange currents. The effects of those currents can be interpreted as pion/meson contributions since they include processes associated with pion exchange and quark-antiquark pairs [37, 38, 39, 40]. This interpretation is also valid in the large N_c limit, where the form factor G_E and the product $\frac{|q|}{2M_\Delta} G_C$ appear as higher orders in $1/N_c$ compared to G_M [33, 67].

For future discussions, it is worth noticing that the $SU(6)/\text{large}N_c$ estimates are based on non relativistic kinematics and therefore may ignore some high angular momentum state effects that emerge in a relativistic framework.

Indications of the dominance of the pion cloud contributions have been found also within the framework of the dynamical coupled-channel models, like the Sato-Lee and the DMT models [7, 30, 31, 32, 41].

It is worth mentioning that eqs. (2)-(3) should not be strictly interpreted as pion cloud contributions, because the empirical parametrization of G_{En} include all possible contributions, including also the effects of the valence quarks. We note, however, that in an exact $SU(6)$ model the contributions from the valence quarks associated with one-body currents vanishes [39, 64, 68, 69]. In a model where the $SU(6)$ symmetry is broken in first approximation, one can expect that the quark-antiquark contributions are the dominant effect in G_{En} and r_n^2 [38, 39]. Examples of models with meson cloud/sea quark dominance can be found in [25, 23, 70, 71, 72]. We conclude then that (2)-(3) can still be used to estimate the pion cloud contribution to the $\gamma^*N \rightarrow \Delta(1232)$ quadrupole form factors in the cases where the valence quark contributions are small.

We assume that eqs. (2)-(3) and in particular the analytic parametrizations of G_{En} hold also for $Q^2 < 0$. This assumption is justified by the smooth behavior inferred for G_{En} based on the empirical data, and also because the range of extrapolation is small, since $Q_{pt}^2 \simeq -0.086 \text{ GeV}^2$. In this range, the effects associated with the timelike pole structure, such as the effects of the ρ -pole ($Q^2 \simeq -0.6 \text{ GeV}^2$), are attenuated, or can be represented in an effective form. In sect. 4.5 we show that G_{En} is in fact dominated, near the pseudothreshold, by the first two terms of the expansion in Q^2 . Note that the two pion production threshold $Q^2 = -4m_\pi^2 \simeq -0.076 \text{ GeV}^2$, the point where the transition form factors become complex functions, is just a bit above the $\gamma^*N \rightarrow \Delta(1232)$ pseudothreshold. Since, according to chiral perturbation theory, the transition to the complex form factors is smooth [55, 56], we can ignore the imaginary component of the form factors in first approximation, and treat the form factors in the timelike region as simple extrapolations of the analytic parametrizations derived in the spacelike region. Similar extrapolations to the timelike region can also be found in [44, 73, 74].

The relations (2)-(3) are derived in [20] and improve previous large N_c relations [33], in order to satisfy Siegert's theorem exactly (1). The main difference between our analytic expressions for the functions G_E^π and G_C^π compared to the expressions derived in [33], is in eq. (2), where we include a denominator in the factor \tilde{G}_{En} . This new factor corresponds to a relative correction $\mathcal{O}(1/N_c^2)$, relative to the original derivation for G_E^π , at the pseudothreshold¹. Using the new form, one obtains at the pseudothreshold: $1 + \frac{Q^2}{2M_\Delta(M_\Delta - M)} = \frac{M_\Delta + M}{2M_\Delta}$, which lead directly to eq. (1). In a previous work [19], an approximated expression was considered for G_E^π , where the error in the description of Siegert's theorem is a term $\mathcal{O}(1/N_c^4)$.

Previous studies of Siegert's theorem based on quark models [16, 43, 75, 76, 77] show that the theorem can be violated when the operators associated with the charge density, or the current density, are truncated in different orders, inducing a violation of the current conservation condition [43]. From those works, we can conclude that, a consistent calculation with current conservation, cannot be reduced to the photon coupling with the individual quarks (one-body currents), since the current is truncated. In those conditions, it is necessary the inclusion of higher-order terms such as two-body currents, in order to ensure current conservation and to be consistent with Siegert's theorem [43]. The description of Siegert's theorem, requires then the inclusion of processes beyond the impulse approximation (one-body currents) [42, 43].

We recall at this point that eqs. (2)-(3) are the result of derivations valid at small Q^2 [33]. For very large values of Q^2 , we expect the pion cloud contributions to be negligible in comparison to the valence quark contributions. Thus, one can assume that for large Q^2 , the equations (2)-

¹ Since in the large N_c limit $M_\Delta - M = \mathcal{O}(1/N_c)$, and $M, M_\Delta = \mathcal{O}(N_c)$, the factor $1/\left(1 + \frac{Q^2}{2M_\Delta(M_\Delta - M)}\right)$ corresponds to a correction $\mathcal{O}(1/N_c^2)$, at the pseudothreshold.

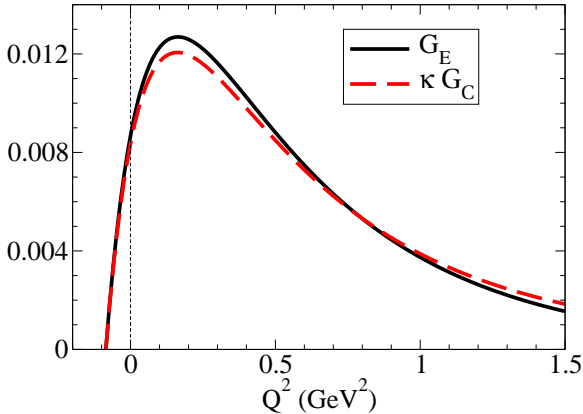


Fig. 1. Valence quark contributions for G_E and G_C according to [18]. Recall that $\kappa = \frac{M_{\Delta} - M}{2M_{\Delta}} \simeq 0.12$.

(3) are corrected according to $G_E^\pi \rightarrow G_E^\pi / (1 + Q^2/\Lambda_E^2)^2$ and $G_C^\pi \rightarrow G_C^\pi / (1 + Q^2/\Lambda_C^2)^4$, where Λ_E and Λ_C are large momentum cutoff parameters [20]. In those conditions, the form factors G_E and G_C are, at large Q^2 , dominated by the valence quark contributions, as predicted by perturbative QCD, with falloffs $G_E \propto 1/Q^4$ and $G_C \propto 1/Q^6$ [78, 79]. The falloffs of the pion cloud components are then $G_E^\pi \propto 1/Q^8$ and $G_C^\pi \propto 1/Q^{10}$, where the extra factor ($1/Q^4$) takes into account the effect of the extra quark-antiquark pair associated with the pion cloud [78, 79].

Adding the valence quark contributions

The pion cloud contributions to the $\gamma^*N \rightarrow \Delta(1232)$ quadrupole form factors given by eqs. (2)-(3) should be complemented by valence quark contributions to the respective form factors. Calculations from quark models estimate that the valence quark contribution to the $\gamma^*N \rightarrow \Delta(1232)$ quadrupole form factors are an order of magnitude smaller than the data [1, 7, 16, 17, 36, 80]. It is known, however, that small valence quark contributions to the quadrupole form factors can help to improve the description of the data [18, 19].

The valence quark contributions to the $\gamma^*N \rightarrow \Delta(1232)$ quadrupole form factors are in general the result of high angular momentum components in the nucleon and/or $\Delta(1232)$ wave functions. The valence quark contributions to the quadrupole form factors vanish at the pseudothreshold, as a consequence of the orthogonality between the nucleon and $\Delta(1232)$ states, as discussed in [19]. In those conditions, the valence quark contributions to the quadrupole form factors play no role in Siegert's theorem, which depends exclusively on the pion cloud contributions. The parameterizations (2)-(3) then ensure that Siegert's theorem is naturally satisfied.

In order to improve the description of the $\gamma^*N \rightarrow \Delta(1232)$ quadrupole form factors, we combine the pion cloud parameterizations (2)-(3) with the valence quark contributions (index B), using $G_a = G_a^B + G_a^\pi$, for $a = E, C$.

For the valence quark contributions we use in particular the quark model from [18], since in this work the valence quark contributions are calculated using an extrapolation from the lattice QCD simulations in the quenched approximation with large pion masses [81]. Recall that in lattice QCD simulations with large pion masses, the meson cloud effects are very small, and the physics associated with the valence quarks can be better calibrated [9, 18, 82]. The free parameters of the model are two D -state admixture coefficients and three momentum scales associated with the radial structure of the D -states. All those parameters are determined accurately by the results from lattice QCD simulations [18]. The chi-square per degree of freedom associated with the fit of the model to the lattice QCD results is 0.58 for G_E and 1.17 for G_C . The number of degrees of freedom of the fit is 37 and the combined chi-square per degree of freedom is 0.76.

The model under discussion is covariant and can therefore be used to estimate the valence quark contributions in any range of Q^2 [18, 60]. The results of the valence quark contributions to the form factors G_E and G_C estimated by the model from [18] are presented in fig. 1. The available data near $Q^2 = 0$ is $G_E(0) = 0.076 \pm 0.015$ and $\kappa G_C(0.04 \text{ GeV}^2) = 0.075 \pm 0.021$ [20, 41, 83]. Based on fig. 1, one can then conclude that the valence quarks contribute only for about 10% of the empirical data near $Q^2 = 0$. The theoretical uncertainties associated with the results from fig. 1 are discussed later on.

Estimates based on the Dyson-Schwinger formalism suggest that relativistic effects, in particular P -state contributions, can increase the magnitude of the valence quark contributions [12, 13]. These results suggest that our estimates of the pion cloud contributions may be overestimated.

3 Parametrizations of G_{En}

The parametrizations of G_{En} can be represented by an expansion near $Q^2 = 0$ in the form [38]:

$$G_{En}(Q^2) \simeq -\frac{1}{6}r_n^2 Q^2 + \frac{1}{120}r_n^4 Q^4 - \frac{1}{5040}r_n^6 Q^6 + \dots, \quad (4)$$

where each term defines a momentum of the function G_{En} . In the previous equation, r_n^2 is the first moment, r_n^4 is the second moment, r_n^6 is the third moment, and so on. The first moment is well known experimentally: $r_n^2 \simeq -0.116 \text{ fm}^2$ [83]. The value of the second moment (r_n^4) controls the curvature of the function G_{En} near $Q^2 = 0$. For r_n^4 , we need, at the moment, to rely on models. A discussion about the possible values for r_n^4 can be found in [38]. The third moment (r_n^6) is usually omitted in the discussions, it can be used to discriminate two close parametrizations.

For the discussion, it is important to present also the form of the most popular parametrization of G_{En} , the Galster parametrization [48, 49, 52]:

$$G_{En}(Q^2) = -\frac{1}{6}r_n^2 \frac{Q^2}{1 + d\tau_n} G_D, \quad (5)$$

where $\tau_N = \frac{Q^2}{4M^2}$, d is a free parameter, and G_D is the nucleon dipole $G_D = 1/(1 + Q^2/\Lambda^2)^2$ with $\Lambda^2 = 0.71 \text{ GeV}^2$. Since r_n^2 is well determined experimentally, there are only two independent parameters in (5), counting Λ as a parameter.

In the present work, we use the following form to parametrize the function \tilde{G}_{En} :

$$\tilde{G}_{En}(Q^2) = \frac{c_0(1 + c_2Q^2 + \dots + c_kQ^{2k-2})}{1 + c_1Q^2 + \frac{c_2^2}{2!}Q^4 + \dots + \frac{c_1^{k+2}}{(k+2)!}Q^{2k+4}}, \quad (6)$$

where $k = 2, 3, \dots$ is an integer and c_l ($l = 0, \dots, k$) are adjustable coefficients. The use of eq. (6) is motivated by the relation between the quadrupole form factors G_E and G_C and the neutron electric form factor G_{En} , and also by previous studies of Siegert's theorem [42]. The parametrizations of the transition form factors are sometimes performed based on analytic forms that are valid only in a limited region of Q^2 . Examples of those representations are the MAID parametrizations, based on polynomials and exponentials [44]. Those representations have problems in the extension for the timelike region (large exponential effects) and in the large- Q^2 region where the form factors have very fast exponential falloffs, instead of power law falloffs predicted by perturbative QCD [78, 79]. Alternatively, the parametrizations based on rational functions can describe both the low- and large- Q^2 regions with the appropriate power law falloffs, and can also be extended to the timelike region. Depending on the resonance under study, the parameter c_1 can be chosen in order to avoid singularities above the pseudothreshold [42]. Note that for large Q^2 , one has $\tilde{G}_{En} \propto 1/Q^6$, as expected from perturbative QCD arguments [78, 79].

The form (6) was used in [42] to parametrize directly the G_C data. A modified form with a different asymptotic falloff was also used to parametrize the G_E data ($G_E \propto 1/Q^4$, for large Q^2). From eq. (6), one can derive the following relations for the first (r_n^2), the second (r_n^4), and the third (r_n^6) moments of G_{En} , as defined in eq. (4):

$$\begin{aligned} c_0 &= -\frac{1}{6}r_n^2, \\ c_0(c_2 - c_1) &= \frac{1}{120}r_n^4, \\ \frac{1}{2}c_0 [c_1(c_1 - c_2) + 2c_3] &= -\frac{1}{5040}r_n^6. \end{aligned} \quad (7)$$

We fix the value of r_n^2 by the experimental value $r_n^2 \simeq -0.116 \text{ fm}^2$ (or -2.98 GeV^{-2}), due to its precision. Typical values for r_n^4 are in the range $r_n^4 = -(0.60-0.30) \text{ fm}^4$ [38, 52, 53]. The third moment is discussed later.

The parametrization (6) has only k independent coefficients: c_l ($l = 1, \dots, k$), because c_0 is fixed by the data. There are then k adjustable parameters.

4 Combined fit of G_{En} , G_E and G_C

In this section, we present the results of the global fit of eqs. (2), (3) and (6) to the G_{En} , G_E and G_C data,

based on the chi-square minimization. Since the pion cloud expressions for G_E and G_C are derived at low Q^2 [33], we restrict the fit of the quadrupole form factors to the $Q^2 < 1.5 \text{ GeV}^2$ region. For G_{En} we consider no restrictions in the data. The quality of the fits is measured by the chi-square value per degree of freedom (reduced chi-square) associated with the different data sets.

We start by discussing the data used in our fits and the explicit form used for G_{En} (sects. 4.1 and 4.2). After that, we present the results for two different cases. First, we consider a simple model where we neglect the effect of the valence quark contributions (sect. 4.3). Next, we present the results of our best fit to the global data, including the valence quark contributions to the $\gamma^*N \rightarrow \Delta(1232)$ quadrupole form factors (sect. 4.4). Once determined our best fit to the global data we discuss the results for G_{En} (sect. 4.5) and the results to the $\gamma^*N \rightarrow \Delta(1232)$ quadrupole form factors (sect. 4.6), including the values obtained for the electric and Coulomb quadrupole square radii (sect. 4.7). At the end, we debate some theoretical and experimental aspects related to the final results.

4.1 Data

In the present work, we consider the data for G_{En} from [54, 84]. The data from [84] are extracted from the analysis of the deuteron quadrupole form factor data, providing data at very low Q^2 . Reference [54] presents a compilation of the data from different double-polarization experiments [85, 86, 87, 88, 89, 90, 91, 92, 93, 94], which measure the ratio G_{En}/G_{Mn} , where G_{Mn} is the neutron magnetic form factor. In total, we consider 35 data points for G_{En} .

Concerning the $\gamma^*N \rightarrow \Delta(1232)$ quadrupole form factor data, we consider a combination of the database from [95], the recent data from JLab/Hall A [41], and the world average of the Particle Data Group for $Q^2 = 0$ [83]. The database from [95] includes data from MAMI [80], MIT-Bates [96] and JLab [97, 98] for finite Q^2 . Comparatively to [95], we replace the G_C data below 0.15 GeV^2 from [80, 96], by the new data from [41]. This procedure was adopted because it was shown that there is a discrepancy between the new data and previous measurements from MAMI and MIT-Bates [80, 96] below 0.15 GeV^2 , due to differences in the extraction procedure of the resonance amplitudes from the measured cross sections [41]. For the same reason, the MAMI data from [99] are not included. As for G_E , we combine the data from [95] with the more recent data from JLab/Hall A [41]. Since we restrict the quadrupole form factor data to the region $Q^2 < 1.5 \text{ GeV}^2$, the G_E data is restricted to 15 data points and the G_C data to 13 data points.

The data for G_E and G_C are converted from the results from [41, 95, 83]. In the case of [95] the form factors G_M , G_E and G_C are calculated from the helicity amplitudes $A_{1/2}$, $A_{3/2}$ and $S_{1/2}$ using standard relations [2, 3, 44]. For $Q^2 = 0$, we use the PDG data [83] for the electromagnetic ratios $R_{EM} \equiv -\frac{G_E}{G_M}$ and $R_{SM} \equiv -\frac{q_1}{2M_\Delta} \frac{G_C}{G_M}$, combined with the experimental value of $G_M(0)$ [44] (\mathbf{q} is

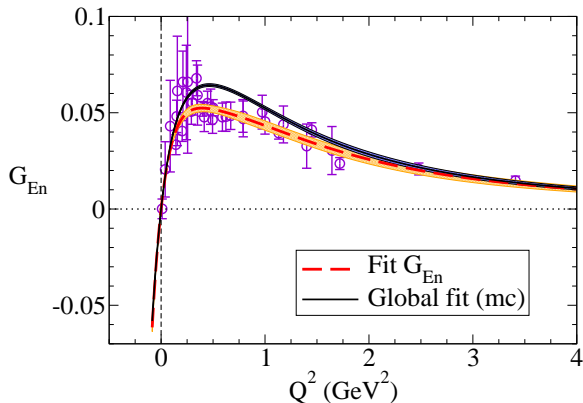


Fig. 2. Neutron electric form factor. Results of the direct fit to the G_{En} data (dashed line, thick band), and of the global fit without the valence quark contributions (thin band). The label “mc” stands for meson cloud. Data from [54,84].

the photon three-momentum in the $\Delta(1232)$ rest frame). As for the recent data from [41] for R_{EM} and R_{SM} , we use the MAID2007 parametrization for G_M , since the helicity amplitudes are not available for all values of Q^2 . The MAID2007 parametrization for G_M can be expressed as $G_M = 3\sqrt{1+\tau}(1+a_1Q^2)e^{-a_4Q^2}$, where $\tau = \frac{Q^2}{(M_\Delta+M)^2}$, $a_1 = 0.01 \text{ GeV}^{-2}$ and $a_4 = 0.23 \text{ GeV}^{-2}$ [44]. The MAID-2007 parametrization provides a very good description of the low- Q^2 data.

4.2 Parametrization for G_{En}

In the calculation of the pion cloud contributions to G_E and G_C , we use the parametrization of G_{En} given by eq. (6), where we take $k = 3$ (3 parameters). Compared to the Galster parametrization (5), we consider one additional parameter. Using eq. (6), we avoid an explicit dependence on the dipole factor G_D . This procedure may be more appropriated for the study of the $\gamma^*N \rightarrow \Delta(1232)$ transition form factors, since it avoids the connection with a scale associated exclusively with the nucleon [19].

Fits based on parametrizations with larger values of k ($k \geq 4$) lead to similar results at low Q^2 , but increase the number of parameters. In addition, for $k \geq 5$, the higher order coefficients c_i of the parametrizations are constrained mainly by the $Q^2 > 2 \text{ GeV}^2$ data, which is restricted to 2 data points (2.48 GeV^2 and 3.41 GeV^2). Those coefficients are therefore poorly constrained, and can lead to strong oscillations in the function G_{En} for large Q^2 , in conflict with the smooth falloff expected for large Q^2 . Parametrizations of G_{En} with $k \geq 5$ may be considered, once more information relative the function G_{En} become available, such as, more and better distributed data at large Q^2 .

4.3 Model with no valence quark contributions

In order to test whether the inclusion of the valence quark effects on the $\gamma^*N \rightarrow \Delta(1232)$ quadrupole form factors is really relevant for the description of the data, we consider first two fits where we ignore those effects.

We start with a direct fit to the G_{En} data, ignoring the impact of the quadrupole form factor data. The parameters associated with the fit and the respective errors are presented in the first row of table 1. The coefficients of correlation between the parameters are also presented in the table and are discussed later. The reduced chi-square associated with the G_{En} fit is 0.66, pronouncing the good quality of fit. The parameters of the global fit to the G_{En} , G_E and C_C data, using only the meson cloud term, and the corresponding errors are presented in the second row of table 1. The values of reduced chi-square associated with the different subsets and the combined chi-square per degree of freedom are presented in the second row of table 2.

From the chi-square values presented in the second row of table 2, one can anticipate that a fit that does not include additional contributions to the pion cloud parametrization lead to a very poor description of the G_C data (reduced chi-square 6.7), as well as an imprecise description of the neutron electric form factor data (reduced chi-square 2.7) and the electric quadrupole form factor data (reduced chi-square 2.0).

The results of the two fits to the G_{En} , including the interval of variation associated with the uncertainties in the parameters are presented in fig. 2. The dashed line represent the result of the fit to the G_{En} data and the uncertainties are represented by the thick band (orange). The thin band represents the result of the global fit (including the uncertainties). The range of the variation of G_{En} is estimated using the propagation of errors associated with the coefficients c_i according to the parametrization (6) with $k = 3$ [100].

In fig. 2, we also present the results below $Q^2 = 0$ down to $Q^2 = -(M_\Delta - M)^2 \simeq -0.09 \text{ GeV}^2$, which correspond to the pseudothreshold of the $\gamma^*N \rightarrow \Delta(1232)$ transition. As mentioned, the region below $Q^2 = 0$ is important for the study of the quadrupole form factors and to Siegert’s theorem [19,20].

The results for the quadrupole form factors, G_E and G_C , are presented in fig. 3. In this case, the interval of variation is small (narrower bands).

The errors associated with the coefficients c_j are determined based on standard relations that take into account the errors associated with the data and the sensibility of the parameters relative to the data. The last effect is estimated by $\left(\frac{\partial c_j}{\partial y_i}\right)$ where y_i represent the G_{En} , G_E or G_C data [100,101]. The available data suggest that the coefficients c_1 , c_2 and c_3 are not really uncorrelated, since the coefficients of correlation between the parameters differ significantly from zero [100,101]. The coefficients of correlation and the covariance functions are presented in the last three columns of table 1. Note in particular that the coefficient of correlation between c_1 and

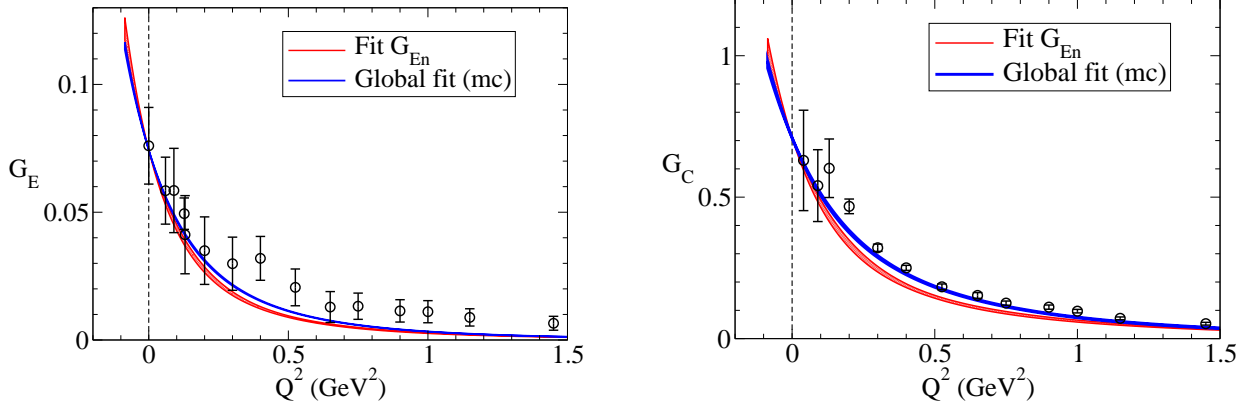


Fig. 3. $\gamma^*N \rightarrow \Delta(1232)$ electric and Coulomb quadrupole form factors. Results of models with no valence quark contributions. Results of the direct fit to the G_{En} data (red band), and the global fit (blue band). The label “mc” stands for meson cloud. Data for proton targets from [41,80,83,96,97,98].

Table 1. Parameters c_i associated with the parametrization from eq. (6) for the case $k = 3$. The brackets represent the uncertainty associated with the parameters. In the first row $\rho_{c_i c_j}$ represents the coefficient of correlation between c_i and c_j . In the second row $\sigma_{c_i c_j}$ represent the covariance between c_i and c_j .

	c_1 (GeV $^{-2}$)	c_2 (GeV $^{-2}$)	c_3 (GeV $^{-4}$)	$\rho_{c_1 c_2}$ $\sigma_{c_1 c_2}$ (GeV $^{-4}$)	$\rho_{c_1 c_3}$ $\sigma_{c_1 c_3}$ (GeV $^{-6}$)	$\rho_{c_2 c_3}$ $\sigma_{c_2 c_3}$ (GeV $^{-6}$)
Fit G_{En}	3.39 (0.39)	-0.750 (0.135)	2.01 (0.77)	0.39 (0.021)	0.97 (0.29)	0.21 (0.025)
Global fit (only meson cloud)	3.31 (0.19)	-0.175 (0.113)	1.71 (0.34)	0.84 (0.019)	0.97 (0.063)	0.69 (0.026)
Global fit (total)	3.28 (0.17)	-0.954 (0.077)	1.93 (0.26)	0.62 (0.0079)	0.95 (0.042)	0.36 (0.0073)
Fit G_{En}, G_E	3.47 (0.42)	-0.744 (0.138)	2.19 (0.90)	0.35 (0.020)	0.98 (0.37)	0.19 (0.015)

c_3 , $\rho_{c_1 c_3}$, is very close to one, indicating a strong correlation between the effect of those two coefficients. A consequence of the correlation between coefficients is that to estimate the range of variation of G_{En} we cannot consider just the quadratic terms $\left(\frac{\partial G_{En}}{\partial c_i}\right)^2 \sigma_{c_i}^2$ associated with c_1 , c_2 and c_3 , but that it is also necessary to consider the cross terms: $2\left(\frac{\partial G_{En}}{\partial c_i}\right)\left(\frac{\partial G_{En}}{\partial c_j}\right)\sigma_{c_i c_j}$, where $\sigma_{c_i c_j}$ is the covariance function between c_i and c_j [100]. The narrow bands presented in the following figures are the consequence of the inclusion of the cross terms.

One can now comment on the results of the fits. In fig. 2, we can notice that the direct fit to the data provide a much better description of the G_{En} data (reduced chi-square 0.66) than the global fit restricted to the meson cloud term (reduced chi-square 2.65). In the last case the fit overestimates the G_{En} data for $Q^2 > 0.25$ GeV 2 . It is worth noticing that, although the combined fit reduces the errors associated with the parameters, and consequently the width of the bands associated with G_{En} , that does not imply that the data description is more accurate, as can be inferred from the reduced chi-square values.

Table 2. Quality of the parametrizations measured in terms of chi-square per degree of freedom (G_{En} , G_E and G_C). $\chi^2(\text{tot})$ is the total chi-square per degree of freedom. The results between brackets indicate the values associated with the sets not included in the fits.

	$\chi^2(G_{En})$	$\chi^2(G_E)$	$\chi^2(G_C)$	$\chi^2(\text{tot})$
Fit G_{En}	0.66	(2.70)	(26.5)	
Global fit (mc)	2.65	2.03	6.73	2.94
Global fit	0.77	0.67	1.15	0.77
Fit G_{En}, G_E	0.66	0.63	(2.33)	

As for the quadrupole form factors displayed in fig. 3, we can conclude that the combined fit (at blue) improves the description of the quadrupole form factor data compared to a fit that excludes those data (at red). The improvement is more significant for G_C . Both fits show a reasonable agreement with the data near $Q^2 = 0$. Focusing on the global fit, it is important to mention that the results are the consequence of the overestimated results for G_{En} , which enhance the values of G_E and G_C at low

Q^2 in about 30%. We can also note that G_E is poorly described for $Q^2 > 0.4 \text{ GeV}^2$ and that the global fit of G_C underestimates the data in the region $Q^2 \approx 0.2 \text{ GeV}^2$.

To summarize this first analysis, one can say that a global fit which neglects the valence quark contributions appears to give a reasonable description of the quadrupole form factor data at low Q^2 . Those results, however, are a consequence of a rough description of the G_{En} data.

4.4 Global fit (including the valence quark contributions)

We consider now a global fit to the data that take into account the contribution of the valence quarks on the quadrupole form factors G_E and G_C . The inclusion of the valence quark term introduces additional uncertainties in the calculations, since there are now uncertainties associated with the quark model estimates of the functions G_a^B ($a = E, C$).

The simplest way of taking into account those uncertainties in the fit it is to modify the experimental standard deviation σ_i associated with G_a according to $\sigma_i^2 \rightarrow \sigma_i^2 + \sigma^2(G_a^B)$, in the chi-square calculation, where $\sigma(G_a^B)$ is the theoretical error associated with the result for G_a^B . The previous modification is justified in the calculation of the factor $G_a - (G_a^B + G_a^\pi)$, when the errors are combined in quadrature. The main consequence of the previous procedure is the reduction of the impact of the G_E and G_C data in the global fit, since the contribution of each term is weighted by the factor $1/\sigma_i^2$. In those conditions the chi-square associated with the experimental data differ from the *effective* chi-square obtained when we include the quark model uncertainties (the model uncertainties reduce the chi-square values). The interpretation of the reduced chi-square values become less clear, then, since it is not restricted exclusively to the experimental data.

For the reasons mentioned above, we choose not to take into account explicitly the uncertainties associated with the quark model in the global fit to the data. Alternatively, we determined the chi-square taking into account the experimental errors and include the quark model uncertainties afterward in the representation of the results for G_E and G_C . With this procedure, we preserve the usual interpretation of reduced chi-square based on the experimental data. The quark model uncertainties are taken into account later in the discussion of the results for the quadrupole form factors.

The parameters associated with the best fit to the G_{En} , G_E and G_C data, including the valence quark and meson cloud contributions on the quadrupole form factors are presented in the third row of table 1. The results for the reduced chi-square associated with the different sets of data are presented in the third row of table 2.

The chi-square values obtained in the global fit seems to suggest that all the data subsets (G_{En} , G_E and G_C) are well described, since the reduced chi-square is smaller than the unit, or just a bit larger, in the case of G_C . One can then conclude that if the theoretical uncertainties

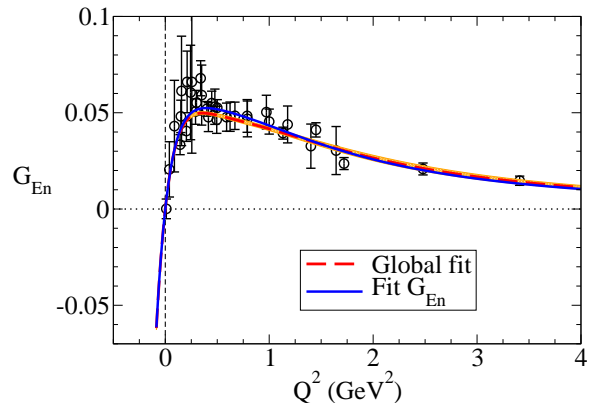


Fig. 4. Neutron electric form factor. Best fit to the data (band and dashed line) compared with the direct fit and with the G_{En} data (solid line). Data from [54, 84].

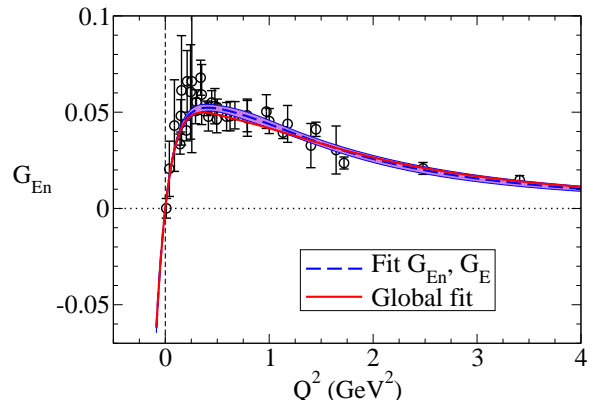


Fig. 5. Neutron electric form factor. Best fit to the data (solid line) compared with the best fit to the G_{En} and G_E data (excluding the G_C data). The bands represent the errors associated with the partial fit (G_{En} and G_E). The errors associated with the global fit are not included for clarity (see fig. 2). Data from [54, 84].

are small, the inclusion of the valence quark contributions improves the global description of the data.

The numerical results for G_{En} and for the quadrupole form factors G_E and G_C are discussed in the following subsections, including the uncertainties associated with the quark model from [18]. The relative uncertainties associated with the quark model can be determined numerically combining the lattice QCD results G_a^{latt} with the model estimate of that result in lattice G_a^B . One conclude then that the errors associated with the functions G_E^B and G_C^B can be expressed² as $\sigma(G_E^B) = 0.45 G_E^B$ and $\sigma(G_C^B) = 0.33 G_C^B$.

² The relative uncertainty of the model for G_a^B is determined by $\frac{\sigma(G_a^B)}{G_a^B}$. We can estimate $\left(\frac{\sigma(G_a^B)}{G_a^B}\right)^2$ using the average $\left\langle \left(\frac{G_a^{\text{latt}} - G_a^B}{G_a^B}\right)^2 \right\rangle$. In the calculation the weight of each point is $1/\sigma^2(G_a^{\text{latt}})$.

The comparison of the results of the quark model with lattice QCD results is possible because the meson cloud effects are suppressed in lattice QCD simulations with large pion masses [18]. The lattice QCD results for G_E and G_C are calculated from the results for G_E/G_M and G_C/G_M , which have uncertainties much larger than G_M . In total one has 21 points for G_E and 21 points for G_C for $m_\pi = 411, 490$ and 593 MeV [18,81].

4.5 Neutron electric form factor (G_{En})

We now discuss the numerical results for G_{En} presented in fig. 4 (solid line) in comparison with the data from [54, 84].

The quality of the description of the G_{En} data and the narrow band of variation can be observed in detail in fig. 4, where we include also the results of the single fit to the G_{En} data, where we neglect the effect if the G_E and G_C data. In the last case, we omit the band of variation associated with the first model (fit G_{En}) for clarity. The comparison with the results from fig. 2 is sufficient to show that the errors associated with the function G_{En} are reduced when we consider the global fit. Based on the results presented in the third row of table 1, one can conclude that the errors associated the parameters decrease compared to the previous fits, justifying the thin band of variation presented in the figure.

The parametrization presented in fig. 4 correspond to the value

$$r_n^4 = (-0.383 \pm 0.012) \text{ fm}^4. \quad (8)$$

This estimate is close to other estimates presented in the literature based on the Galster parametrization [38] and similar parametrizations [53]. For the purpose of the discussion, we note that a Galster parametrization that provides a good description of the G_{En} data, associated with $d = 2.8$ correspond to $r_n^4 \simeq -0.30 \text{ fm}^4$ [19,20,37].

It is also worth mentioning that in a parametrization that include the factor G_D , a significant contribution to r_n^4 comes from a term on $1/\Lambda^2$, where $\Lambda^2 = 0.71 \text{ GeV}^2$. When we consider a Galster parametrization, the last contribution is about -0.25 fm^4 . It is then interesting to conclude that we obtain a result close to the Galster parametrization, without including the factor G_D .

The comparison between the results for the third moment is even more compelling. We obtain almost the same result for r_n^6 : $r_n^6 = (-1.31 \pm 0.12) \text{ fm}^6$, using the parametrization with rational functions and $r_n^6 \simeq -1.34 \text{ fm}^6$, using the Galster parametrization with $d = 2.8$ [19,20,37]. We conclude then that the two parametrizations are distinguished near $Q^2 = 0$, within the uncertainties, basically by the value of the second moment (r_n^4).

In figs. 2 and 4, we can notice that the different parametrizations have a very similar extension to the timelike region, including the pseudothreshold. Very similar results can also be obtained with the Galster parametrization. This effect is explained by the dominance of the first two terms (first and second moments) in the expansion of G_{En} from (4) near the pseudothreshold.

In order to test the dependence of the fit on the data subsets, we perform also partial fits to the combination of the data (G_{En}, G_E) and (G_{En}, G_C). This way, we test which quadrupole set, G_E or G_C , has more impact in the global fit, and we can also infer if those sets are compatible with the G_{En} data. The result of the fit to the sets (G_{En}, G_C) is represented in fig. 5 by the blue band. The global fit (G_{En}, G_E and G_C) is represented by the solid line. The result of the combined fit for (G_{En}, G_C) is almost undistinguished from the global fit (solid line), and it is not presented for clarity. The parameters associated with the partial fit (G_{En}, G_E) are presented in the last row of table 1. Compared to the global fit, we notice the increasing errors associated with the parameters. The corresponding values for the reduced chi-square are presented in the last row of table 2. From the result for $\chi^2(G_C)$ we can confirm that the quality of the description of the G_{En} and G_E is obtained at the expenses of a poorer description of the G_C data.

In the literature, there is some debate whether there is a bump in the function G_{En} near $Q^2 = 0.2-0.3 \text{ GeV}^2$, or not [33,50]. We conclude that the present accuracy of the data is insufficient for more definitive conclusions. Our best fit has a smooth behavior in the region under discussion. Nevertheless, larger values of k can in principle generate a low- Q^2 bump, once one has more high Q^2 data to constrain the higher order coefficients.

When we take into account the theoretical uncertainties associated with the quark model the results for G_{En} are only somewhat modified. The magnitude of G_{En} is slightly enhanced near $Q^2 = 0.5 \text{ GeV}^2$.

4.6 Quadrupole form factors (G_E, G_C)

The results of the best global fit to the $\gamma^*N \rightarrow \Delta(1232)$ quadrupole form factors (solid line) including the theoretical uncertainties (orange band) are presented in fig. 6, in comparison with the respective data. For comparison, we include also the previous fit where we ignore the valence quark contributions (dashed line).

Focusing first in the central values (solid line) we observe an excellent agreement with the data in the range $Q^2 = 0-1.5 \text{ GeV}^2$, for both form factors. As mentioned before, the quality of the description is corroborated by the reduced chi-square values presented in table 2, 0.67 and 1.15 for G_E and G_C , respectively. For this agreement contributes the larger error bars for the data below 0.2 GeV^2 . The precision of the $Q^2 < 0.2 \text{ GeV}^2$ data is comparable to the precision of most of the neutron electric form factor data. We note, however, that in the present case it is not sufficient to look for the chi-square values, because there are also uncertainties associated with the valence quark contributions.

The uncertainties displayed in fig. 6 are the combination of the pion cloud uncertainties associated with the G_{En} parametrization and the uncertainties associated with the quark model. The main contribution comes from the quark model. The magnitude of the pion cloud uncertainties can be inferred from fig. 3. The uncertainties are

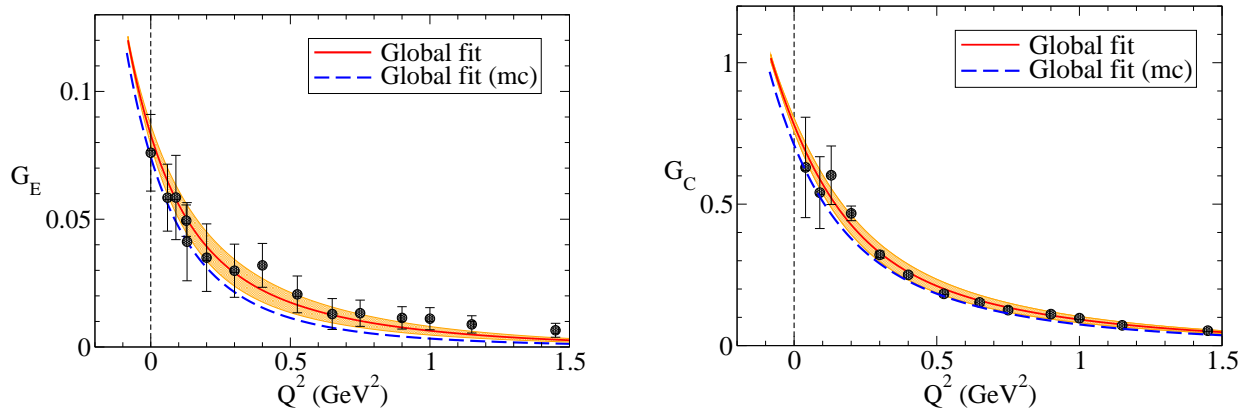


Fig. 6. $\gamma^*N \rightarrow \Delta(1232)$ electric and Coulomb quadrupole form factors. Best global fit to the data (solid line, orange band). The result of the best fit without valence quark contributions is also presented (dashed line, “mc” stands for meson cloud) for comparison. Data for proton targets from [41, 80, 83, 96, 97, 98].

very small at pseudothreshold because according to our estimate, the uncertainties associated with the valence quark contribution vanish and only the pion cloud component contributes (recall that G_E^B and G_C^B vanish at pseudothreshold).

The results from fig. 6 shows that there is a range of variation of G_E^B and G_C^B which give a better solution than models with no valence quark contributions. In the figure, we can notice that the model with no valence quark contributions (dashed line) is a bit below the lower limit of the estimate with valence quark contributions. One can then conclude that the inclusion of the bare contribution improves the description of the data.

The lower limit of the results for G_E is obtained for a bare contribution of about $0.55 G_E^B$, where G_E^B is the estimate of the covariant spectator quark model. In this case, we cannot conclude much, since theoretical and experimental uncertainties are both large and compatible.

The improvement is more significant in the case of G_C with a much narrower band of variation. In this case, the model uncertainties are about 33% of the model estimate G_C^B . One can notice in this case, that although the fit with no valence quark component (dashed line) is just a bit below the lower limit of the model estimate, the reduced chi-square values are very different (see table 2). The difference between those values is a consequence of the small error bars associated with the $Q^2 > 0.2$ GeV² data for G_C . One concludes, then that G_C is more sensitive to the inclusion of the valence quark component.

The comparison of results of G_E with G_C corrected by the factor κ is presented in fig. 7. For clarity, we omit the uncertainties associated with both form factors. In this representation, it is more explicit the connection between the two quadrupole form factors and the implications of Siegert’s theorem. The convergence of the results at the pseudothreshold ($Q^2 \simeq -0.09$ GeV²), the consequence of Siegert’s theorem, is clearly displayed in the graph.

In comparison with the results from [20], where G_{En} is described by a Galster parametrization ($d = 2.8$), we ob-

tain slightly larger values for the quadrupole form factors at the pseudothreshold.

Based on the results of G_E and G_C at $Q^2 = 0$, one can test the accuracy of the large N_c estimate $G_E = \frac{M_\Delta^2 - M^2}{4M_\Delta^2} G_C$, apart $\mathcal{O}(\frac{1}{N_c^2})$ relative corrections [33]. The previous relation is equivalent to the identity $R_{EM}(0) = R_{SM}(0)$ [20, 33]. According to the results from figs. 6 and 7, one obtains $G_E(0) = 0.083 \pm 0.003$ and $\frac{M_\Delta^2 - M^2}{4M_\Delta^2} G_C(0) = 0.082 \pm 0.004$, in agreement with the large N_c prediction, within the uncertainties.

4.7 Square radii r_E^2 and r_C^2

The difference of behavior between the two quadrupole form factors can be better understood when we look at the square radius associated with the quadrupole form factors G_E and G_C , defined by [39, 42, 102]

$$r_a^2 = - \frac{14}{G_a(0)} \left. \frac{dG_a}{dQ^2} \right|_{Q^2=0} \quad (9)$$

where $a = E, C$. The numerical results for r_E^2 and r_C^2 for the parametrizations discussed here are presented in table 3.

If we ignore the effect of the valence quarks, one can calculate r_E^2 and r_C^2 very easily using eq. (2)-(3). One obtains then $r_E^2 = \frac{7}{10} \frac{r_n^4}{r_n^2} + \frac{7}{M_\Delta(M_\Delta - M)}$ and $r_C^2 = \frac{7}{10} \frac{r_n^4}{r_n^2}$. We conclude then that $r_E^2 - r_C^2$ is of order N_c^0 , and it is not suppressed in the large N_c limit. The relation for r_C^2 was derived previously in [39], assuming the dominance of the pion cloud contribution. Using the result (8) for r_n^4 , one obtains the estimates $r_E^2 = 3.06 \pm 0.07$ fm² and $r_C^2 = 2.31 \pm 0.07$ fm². The uncertainties in the previous results are the consequence of the results for r_n^4 , affected by the errors associated with the parametrization G_{En} . Both estimates are about 10% larger than the results for the pion cloud contribution presented in table 3, and are

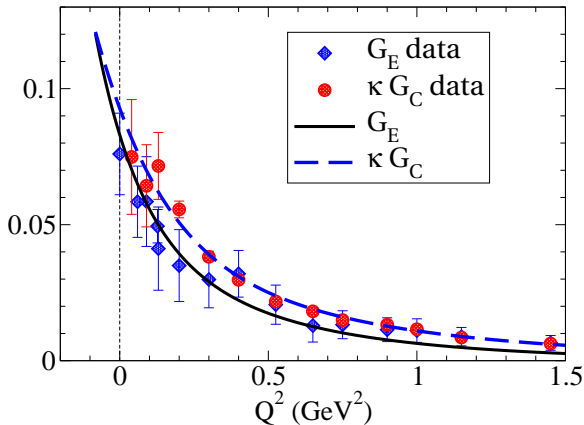


Fig. 7. Results for the form factors G_E and G_C . Recall that $\kappa = \frac{M_\Delta - M}{2M_\Delta} \simeq 0.12$. Data for proton targets from [41, 80, 83, 96, 97, 98].

therefore consistent with a 10% correction for both form factors near $Q^2 = 0$, due to the inclusion of the valence quark contributions, as discussed in sect. 2.

Combining the analytic expressions described previously for r_E^2 and r_C^2 , one has $r_E^2 - r_C^2 = \frac{7}{M_\Delta(M_\Delta - M)} \simeq 0.75$ fm². Note that this result is independent of the general form used for the function G_{En} , and therefore independent of r_n^4 .

The previous estimate differs from the result presented in table 3, mostly because of the valence quark effects are not taken into account as discussed above (10% reduction). Correcting the previous result with the valence quark effect, assuming the 10% correction, one obtains then $(r_E^2 - r_C^2)_\pi \simeq 0.68$ fm². The subindex was included to emphasize that the estimate concerns the pion cloud component. The previous estimate is still in disagreement with the result from table 3, in about -0.04 fm². In this discussion, we omit the uncertainties and focus on the results obtained with the central values presented in the table.

To understand the small difference of -0.04 fm², we need to look into the details of the calculation, and for the very small deviations from the 10% correction, assumed for the valence quark component. If we consider deviation of δ_E and δ_C from the 10% correction to the form factors G_E and G_C , respectively, we conclude that the residual correction can be expressed as $0.9^2(\delta_C - \delta_E)r_{E0}^2$, where the first factor accounts for the 10% correction in the normalizations, and r_{E0}^2 is the estimate of r_E^2 in a model with pion cloud dominance, mentioned above. Combining all effects with $r_{E0}^2 \simeq 3.06$ fm², one obtain $0.9^2(\delta_C - \delta_E)r_{E0}^2 \simeq -0.04$ fm², which explain at last the result $(r_E^2 - r_C^2)_\pi \simeq 0.64$ fm². The last correction is then the consequence of the product of a very small factor by a large factor (r_{E0}^2).

The contributions from the valence quark component depend on the details of the quark model, and are therefore model dependent. Using the model described previously, we obtain $(r_E^2 - r_C^2)_B \simeq -0.06$ fm², where B la-

Table 3. Contributions to the quadrupole square radius (bare and pion cloud): r_E^2 , r_C^2 and difference $r_E^2 - r_C^2$. The results between brackets indicate the uncertainties.

	r_E^2 (fm ²)	r_C^2 (fm ²)	$r_E^2 - r_C^2$ (fm ²)
B	-0.410	-0.347	-0.063
π	(0.169)	(0.107)	(0.200)
	(0.080)	(0.064)	(0.102)
Total	2.331	1.752	0.580
	(0.187)	(0.134)	(0.225)

bels the bare contribution. Combining the two contributions, we obtain $r_E^2 - r_C^2 \simeq 0.58$ fm², as presented in table 3. When we take into account all the errors we obtain $r_E^2 - r_C^2 = 0.58 \pm 0.23$ fm² (see table 3).

Smaller values for r_C^2 have been suggested by empirical parametrizations of the quadrupole form factor data consistent with Siegert's theorem [19, 42]. We note, however, that those estimates are strongly affected by the $Q^2 = 0$ –0.15 GeV² data for G_C , from [80, 96, 99]. Therefore, the conclusions based on those data have to be reviewed in light of the new data from [41].

An important conclusion of the previous discussion is that in order to obtain a reliable estimate of r_E^2 and r_C^2 from the G_E and G_C data, we need more accurate measurements from G_E and G_C near $Q^2 = 0$.

Overall, we can conclude that the large values obtained for r_E^2 and r_C^2 are the outcome of the pion cloud dominance. The magnitudes of r_E^2 and r_C^2 around 2 fm² can be interpreted physically, as the result of the increment of the size of the constituent quarks due to the $q\bar{q}$ pair/pion cloud dressing [39, 42]. More specifically, those magnitudes can be understood looking at the pion Compton scattering wavelength, $r_\pi \approx 1/m_\pi$, which characterize the pion distribution inside the nucleon [39]. Numerically, the result $r_E^2 \approx r_C^2 \approx 2$ fm² is then the consequence of $r_E^2 \approx r_C^2 \approx r_\pi^2$. A more detailed discussion on this subject can be found in [39].

Concerning the difference $r_E^2 - r_C^2 = 0.6 \pm 0.2$ fm², one can conclude that it is mainly a consequence of Siegert's theorem, since the difference between r_E^2 and r_C^2 is the consequence of the extra factor included in the pion cloud parametrization G_E^π , in order to satisfy Siegert's theorem.

4.8 General discussion

Once presented our final results for the neutron electric form factor and for $\gamma^*N \rightarrow \Delta(1232)$ quadrupole form factors, one can discuss some theoretical and experimental aspects related to the present results.

For the good agreement between the model and the data for the quadrupole form factors, displayed in figs. 6 and 7 contributes the valence quark component estimated with a covariant quark model. We stress that this part of the calculation is model dependent and it is then limited by some theoretical uncertainties. Those uncertain-

ties are larger in the case of the electric form factor G_E . Alternative estimates of the valence quark contribution, with the same sign, can also improve the description of the quadrupole form factor data. An example is the bare parametrization of the Sato-Lee model in the $Q^2 > 0$ region [18,32]. Another example is the estimates based on the Dyson-Schwinger formalism, which are expected to be closer to the upper limit of the present calculation.

A test to the valence quark contributions can be performed in a near future with lattice QCD simulations in the range of $m_\pi = 0.2\text{--}0.3$ GeV [103], a region close the physical point, but where hopefully the pion cloud contamination is small. The increase of the number of lattice QCD simulations and of the accuracy of those simulations can also help to improve the accuracy of the present quark model estimates.

Another relevant point of discussion is the accuracy of the data. The data associated with G_{En} have in general large error bars, which difficult the derivation of an accurate parametrization. The G_E and G_C data below 0.15 GeV² are also affected by large error bars. In that region the experimental uncertainties are larger than the quark model uncertainties. For all those reasons it is not hard to find parametrizations that provides a good description of the overall data, including the low- Q^2 region (small chi-square). The inclusion of the G_E and G_C data provide, however, additional constraints to the function G_{En} , which help to pin down the shape of G_{En} .

Another important aspect of the present work is the sensitivity of the fits to the data, particularly in the region $Q^2 = 0\text{--}0.2$ GeV². This effect can be illustrated by the realization that the trend of the function G_C changed with the more recent data [41]. A fit that includes the G_C data from [80,96] cannot describe the data with the same accuracy as a fit that include the more recent data [19]. In conclusion, new data for G_C have also a significant impact on the solution for G_{En} .

To finish the present discussion, we note that we can also test the results of the functions G_E and G_C combining lattice QCD results with estimates based on expansions on the pion mass, derived from effective field theories [104, 105,106]. In these conditions the consistency between the results from lattice QCD and the experimental data can be checked, and therefore, the consistency between QCD and the real world.

5 Outlook and conclusions

In the present work, we derive a global parametrization of the neutron electric form factor and the $\gamma^*N \rightarrow \Delta(1232)$ quadrupole form factors, G_E and G_C . To relate the pion cloud contribution to G_E and G_C with the neutron electric form factor we use improved relations derived in the large N_c limit in order to verify Siegert's theorem exactly.

The success of the global parametrization of G_{En} , G_E and G_C is an indication of the importance of the pion cloud in the neutron and in the $\gamma^*N \rightarrow \Delta(1232)$ transition. This correlation is suggested by the large N_c limit, by

the $SU(6)$ symmetry breaking, and by calculations based on non relativistic constituent quark models.

For the agreement between the model calculations and the empirical data for the $\gamma^*N \rightarrow \Delta(1232)$ quadrupole form factors also contribute the small valence quark components estimated by a covariant quark model, calibrated previously by the results of lattice QCD simulations. Although limited by some model uncertainties, the estimates of the valence quark contributions improve the description of the data compared to models with no bare contributions. Estimates of the valence quark effects based on other frameworks may also improve the description of the $\gamma^*N \rightarrow \Delta(1232)$ quadrupole form factors.

The global fit of the G_{En} , G_E and G_C data, based on rational functions, show that the overall data, and the G_{En} data, in particular, is compatible with a smooth description of the neutron electric form factor with no pronounced bump at low Q^2 . The best description of the data is obtained when we consider a parametrization of G_{En} associated with $r_n^4 = -0.38 \pm 0.01$ fm⁴.

We conclude that the square radii associated with the quadrupole form factors G_E and G_C are large, as a consequence of the pion cloud effects (long extension of the pion cloud). We also conclude that the square radii, r_E^2 and r_C^2 are constrained by the relation $r_E^2 - r_C^2 = 0.6 \pm 0.2$ fm². The previous relation is a consequence of Siegert's theorem and of the dominance of the pion cloud contributions on the quadrupole form factors G_E and G_C .

The present parametrization of the neutron electric form factor is still derived from data with significant error bars below 0.2 GeV². Future experiments with more accurate data for G_{En} , and the $\gamma^*N \rightarrow \Delta(1232)$ quadrupole form factors can help to elucidate the shape of the function G_{En} at low Q^2 . Of particular interest are the upcoming results of the JLab 12-GeV upgrade [1,36].

Acknowledgments

The author thanks Mauro Giannini for helpful discussions. This work was supported by the Fundação de Amparo à Pesquisa do Estado de São Paulo (FAPESP): project no. 2017/02684-5, grant no. 2017/17020-BCO-JP.

References

1. I. G. Aznauryan *et al.*, Int. J. Mod. Phys. E **22**, 1330015 (2013) [arXiv:1212.4891 [nucl-th]].
2. V. Pascalutsa, M. Vanderhaeghen and S. N. Yang, Phys. Rept. **437**, 125 (2007) [hep-ph/0609004].
3. I. G. Aznauryan and V. D. Burkert, Prog. Part. Nucl. Phys. **67**, 1 (2012) [arXiv:1109.1720 [hep-ph]].
4. H. F. Jones and M. D. Scadron, Annals Phys. **81**, 1 (1973).
5. M. A. B. Beg, B. W. Lee and A. Pais, Phys. Rev. Lett. **13**, 514 (1964).
6. C. Becchi and G. Morpurgo, Phys. Lett. **17**, 352 (1965).
7. B. Julia-Diaz, T.-S. H. Lee, T. Sato and L. C. Smith, Phys. Rev. C **75**, 015205 (2007) [nucl-th/0611033].

8. G. Ramalho, M. T. Peña and F. Gross, *Eur. Phys. J. A* **36**, 329 (2008) [arXiv:0803.3034 [hep-ph]].
9. G. Ramalho and M. T. Peña, *J. Phys. G* **36**, 115011 (2009) [arXiv:0812.0187 [hep-ph]].
10. G. Ramalho and K. Tsushima, *Phys. Rev. D* **87**, 093011 (2013) [arXiv:1302.6889 [hep-ph]].
11. G. Ramalho and K. Tsushima, *Phys. Rev. D* **88**, 053002 (2013) [arXiv:1307.6840 [hep-ph]].
12. G. Eichmann and D. Nicmorus, *Phys. Rev. D* **85**, 093004 (2012) [arXiv:1112.2232 [hep-ph]].
13. J. Segovia, C. Chen, C. D. Roberts and S. Wan, *Phys. Rev. C* **88**, 032201 (2013) [arXiv:1305.0292 [nucl-th]].
14. H. Sanchis-Alepuz, R. Alkofer and C. S. Fischer, *Eur. Phys. J. A* **54**, 41 (2018) [arXiv:1707.08463 [hep-ph]].
15. N. Isgur, G. Karl and R. Koniuk, *Phys. Rev. D* **25**, 2394 (1982).
16. S. Capstick and G. Karl, *Phys. Rev. D* **41**, 2767 (1990).
17. G. Ramalho, M. T. Peña and F. Gross, *Phys. Rev. D* **78**, 114017 (2008) [arXiv:0810.4126 [hep-ph]].
18. G. Ramalho and M. T. Peña, *Phys. Rev. D* **80**, 013008 (2009) [arXiv:0901.4310 [hep-ph]].
19. G. Ramalho, *Phys. Rev. D* **94**, 114001 (2016) [arXiv:1606.03042 [hep-ph]].
20. G. Ramalho, *Eur. Phys. J. A* **54**, 75 (2018) [arXiv:1709.07412 [hep-ph]].
21. S. L. Glashow, *Physica A* **96**, 27 (1979).
22. A. M. Bernstein, *Eur. Phys. J. A* **17**, 349 (2003) [hep-ex/0212032].
23. A. J. Buchmann, E. Hernandez and A. Faessler, *Phys. Rev. C* **55**, 448 (1997) [nucl-th/9610040].
24. M. I. Krivoruchenko and M. M. Giannini, *Phys. Rev. D* **43**, 3763 (1991).
25. A. J. Buchmann and E. M. Henley, *Phys. Rev. C* **63**, 015202 (2000) [arXiv:hep-ph/0101027].
26. G. Ramalho, M. T. Peña and A. Stadler, *Phys. Rev. D* **86**, 093022 (2012) [arXiv:1207.4392 [nucl-th]].
27. G. Ramalho, M. T. Peña and F. Gross, *Phys. Lett. B* **678**, 355 (2009) [arXiv:0902.4212 [hep-ph]].
28. G. Ramalho, M. T. Peña and F. Gross, *Phys. Rev. D* **81**, 113011 (2010) [arXiv:1002.4170 [hep-ph]].
29. L. Tiator, D. Drechsel, S. Kamalov, M. M. Giannini, E. Santopinto and A. Vassallo, *Eur. Phys. J. A* **19**, 55 (2004) [nucl-th/0310041].
30. S. S. Kamalov and S. N. Yang, *Phys. Rev. Lett.* **83**, 4494 (1999) [nucl-th/9904072].
31. S. S. Kamalov, S. N. Yang, D. Drechsel, O. Hanstein and L. Tiator, *Phys. Rev. C* **64**, 032201 (2001) [nucl-th/0006068].
32. T. Sato and T. S. H. Lee, *Phys. Rev. C* **63**, 055201 (2001) [nucl-th/0010025].
33. V. Pascalutsa and M. Vanderhaeghen, *Phys. Rev. D* **76**, 111501 (2007) [arXiv:0711.0147 [hep-ph]].
34. M. Fiolhais, B. Golli and S. Širca, *Phys. Lett. B* **373**, 229 (1996) [hep-ph/9601379].
35. D. H. Lu, A. W. Thomas and A. G. Williams, *Phys. Rev. C* **55**, 3108 (1997) [nucl-th/9612017].
36. G. Ramalho, *Few Body Syst.* **59**, 92 (2018) [arXiv:1801.01476 [hep-ph]].
37. A. J. Buchmann, *Phys. Rev. Lett.* **93**, 212301 (2004) [hep-ph/0412421].
38. P. Grabmayr and A. J. Buchmann, *Phys. Rev. Lett.* **86**, 2237 (2001) [hep-ph/0104203].
39. A. J. Buchmann, *Can. J. Phys.* **87**, 773 (2009) [arXiv:0910.4747 [physics.atom-ph]].
40. A. J. Buchmann, J. A. Hester and R. F. Lebed, *Phys. Rev. D* **66**, 056002 (2002) [hep-ph/0205108].
41. A. Blomberg *et al.*, *Phys. Lett. B* **760**, 267 (2016) [arXiv:1509.00780 [nucl-ex]].
42. G. Ramalho, *Phys. Rev. D* **93**, 113012 (2016) [arXiv:1602.03832 [hep-ph]].
43. A. J. Buchmann, E. Hernandez, U. Meyer and A. Faessler, *Phys. Rev. C* **58**, 2478 (1998).
44. D. Drechsel, S. S. Kamalov and L. Tiator, *Eur. Phys. J. A* **34**, 69 (2007) [arXiv:0710.0306 [nucl-th]].
45. L. Tiator and S. Kamalov, *AIP Conf. Proc.* **904**, 191 (2007) [nucl-th/0610113].
46. L. Tiator, *Few Body Syst.* **57**, 1087 (2016).
47. G. Ramalho, *Phys. Lett. B* **759**, 126 (2016) [arXiv:1602.03444 [hep-ph]].
48. S. Galster, H. Klein, J. Moritz, K. H. Schmidt, D. Wegener and J. Bleckwenn, *Nucl. Phys. B* **32**, 221 (1971).
49. J. J. Kelly, *Phys. Rev. C* **66**, 065203 (2002) [hep-ph/0204239].
50. J. Friedrich and T. Walcher, *Eur. Phys. J. A* **17**, 607 (2003) [hep-ph/0303054].
51. W. Bertozzi, J. Friar, J. Heisenberg and J. W. Negele, *Phys. Lett.* **41B**, 408 (1972).
52. S. Platchkov *et al.*, *Nucl. Phys. A* **510**, 740 (1990).
53. M. M. Kaskulov and P. Grabmayr, *Eur. Phys. J. A* **19**, 157 (2004) [nucl-th/0308015].
54. T. R. Gentile and C. B. Crawford, *Phys. Rev. C* **83**, 055203 (2011).
55. N. Kaiser, *Phys. Rev. C* **68**, 025202 (2003) [nucl-th/0302072].
56. M. A. Belushkin, H.-W. Hammer and U.-G. Meissner, *Phys. Rev. C* **75**, 035202 (2007) [hep-ph/0608337].
57. H. W. Hammer and U. G. Meissner, *Eur. Phys. J. A* **20**, 469 (2004) [hep-ph/0312081].
58. I. T. Lorenz, H.-W. Hammer and U. G. Meissner, *Eur. Phys. J. A* **48**, 151 (2012) [arXiv:1205.6628 [hep-ph]].
59. G. Eichmann and G. Ramalho, *Phys. Rev. D* **98**, 093007 (2018) [arXiv:1806.04579 [hep-ph]].
60. F. Gross, G. Ramalho and M. T. Peña, *Phys. Rev. C* **77**, 015202 (2008) [nucl-th/0606029].
61. N. Isgur, G. Karl and D. W. L. Sprung, *Phys. Rev. D* **23**, 163 (1981).
62. N. Isgur and G. Karl, *Phys. Rev. D* **19**, 2653 (1979) Erratum: [*Phys. Rev. D* **23**, 817 (1981)].
63. N. Isgur and G. Karl, *Phys. Rev. D* **20**, 1191 (1979).
64. G. Dillon and G. Morpurgo, *Phys. Lett. B* **448**, 107 (1999).
65. A. J. Buchmann and E. M. Henley, *Phys. Rev. D* **65**, 073017 (2002).
66. A. J. Buchmann and R. F. Lebed, *Phys. Rev. D* **62**, 096005 (2000) [hep-ph/0003167].
67. E. E. Jenkins, X. Ji and A. V. Manohar, *Phys. Rev. Lett.* **89**, 242001 (2002) [hep-ph/0207092].
68. D. B. Lichtenberg, *Unitary Symmetry and Elementary Particles*, (Academic Press, New York, 1978).
69. F. E. Close, *An Introduction to Quarks and Partons*, (Academic Press, London 1979).
70. A. Buchmann, E. Hernandez and K. Yazaki, *Phys. Lett. B* **269**, 35 (1991).
71. C. V. Christov, A. Blotz, H. C. Kim, P. Pobylitsa, T. Watabe, T. Meissner, E. Ruiz Arriola and K. Goeke, *Prog. Part. Nucl. Phys.* **37**, 91 (1996) [hep-ph/9604441].

72. D. H. Lu, A. W. Thomas and A. G. Williams, Phys. Rev. C **57**, 2628 (1998) [nucl-th/9706019].
73. L. Tiator and S. Kamalov, AIP Conf. Proc. **904**, 191 (2007) [nucl-th/0610113].
74. L. Tiator, D. Drechsel, S. S. Kamalov and M. Vanderhaeghen, Eur. Phys. J. ST **198**, 141 (2011).
75. D. Drechsel and M. M. Giannini, Phys. Lett. **143B**, 329 (1984).
76. M. Weyrauch and H. J. Weber, Phys. Lett. B **171**, 13 (1986) [Phys. Lett. B **181**, 415 (1986)].
77. M. Bourdeau and N. C. Mukhopadhyay, Phys. Rev. Lett. **58**, 976 (1987).
78. C. E. Carlson and N. C. Mukhopadhyay, Phys. Rev. Lett. **81**, 2646 (1998) [hep-ph/9804356].
79. C. E. Carlson, Phys. Rev. D **34**, 2704 (1986).
80. S. Stave *et al.* [A1 Collaboration], Phys. Rev. C **78**, 025209 (2008) [arXiv:0803.2476 [hep-ex]].
81. C. Alexandrou, G. Koutsou, H. Neff, J. W. Negele, W. Schroers and A. Tsapalis, Phys. Rev. D **77**, 085012 (2008) [arXiv:0710.4621 [hep-lat]].
82. G. Ramalho, K. Tsushima and F. Gross, Phys. Rev. D **80**, 033004 (2009) [arXiv:0907.1060 [hep-ph]].
83. K. A. Olive *et al.* [Particle Data Group Collaboration], Chin. Phys. C **38**, 090001 (2014).
84. R. Schiavilla and I. Sick, Phys. Rev. C **64**, 041002 (2001) [arXiv:nucl-ex/0107004].
85. T. Eden *et al.*, Phys. Rev. C **50**, 1749 (1994).
86. I. Passchier *et al.*, Phys. Rev. Lett. **82**, 4988 (1999) [arXiv:nucl-ex/9907012].
87. C. Herberg *et al.*, Eur. Phys. J. A **5**, 131 (1999).
88. D. I. Glazier *et al.*, Eur. Phys. J. A **24**, 101 (2005) [arXiv:nucl-ex/0410026].
89. J. Bermuth *et al.*, Phys. Lett. B **564**, 199 (2003) [nucl-ex/0303015].
90. H. Zhu *et al.* [E93026 Collaboration], Phys. Rev. Lett. **87**, 081801 (2001) [arXiv:nucl-ex/0105001].
91. R. Madey *et al.* [E93-038 Collaboration], Phys. Rev. Lett. **91**, 122002 (2003) [arXiv:nucl-ex/0308007].
92. G. Warren *et al.* [Jefferson Lab E93-026 Collaboration], Phys. Rev. Lett. **92**, 042301 (2004) [arXiv:nucl-ex/0308021].
93. E. Geis *et al.* [BLAST Collaboration], Phys. Rev. Lett. **101**, 042501 (2008) [arXiv:0803.3827 [nucl-ex]].
94. S. Riordan *et al.*, Phys. Rev. Lett. **105**, 262302 (2010) [arXiv:1008.1738 [nucl-ex]].
95. V. I. Mokeev, https://userweb.jlab.org/~mokeev/resonance_elec
96. N. F. Sparveris *et al.* [OOPS Collaboration], Phys. Rev. Lett. **94**, 022003 (2005).
97. J. J. Kelly *et al.*, Phys. Rev. C **75**, 025201 (2007) [nucl-ex/0509004].
98. I. G. Aznauryan *et al.* [CLAS Collaboration], Phys. Rev. C **80**, 055203 (2009) [arXiv:0909.2349 [nucl-ex]].
99. N. Sparveris *et al.*, Eur. Phys. J. A **49**, 136 (2013) [arXiv:1307.0751 [nucl-ex]].
100. J. R. Taylor, *An introduction to the Error Analysis*, ch. 9. University Science Books (1997).
101. W. H. Press, S. A. Teukolsky, W. T. Vetterling and B. P. Flannery, *Numerical Recipes in FORTRAN: The Art of Scientific Computing*, ch. 15. Press Syndicate of the University of Cambridge (1997).
102. T. De Forest, Jr. and J. D. Walecka, Adv. Phys. **15**, 1 (1966).
103. C. Alexandrou, G. Koutsou, J. W. Negele, Y. Proestos and A. Tsapalis, Phys. Rev. D **83**, 014501 (2011) [arXiv:1011.3233 [hep-lat]].
104. V. Pascalutsa and M. Vanderhaeghen, Phys. Rev. Lett. **95**, 232001 (2005) [hep-ph/0508060].
105. T. A. Gail and T. R. Hemmert, Eur. Phys. J. A **28**, 91 (2006) [nucl-th/0512082].
106. M. Hilt, T. Bauer, S. Scherer and L. Tiator, Phys. Rev. C **97**, 035205 (2018) [arXiv:1712.08904 [nucl-th]].